JOURNAL OF SPACECRAFT AND ROCKETS
Vol. 35, No. 4, July–August 1998

Motion Control of Adaptive Space Structures Based on Artificial Potential Method

Yuji Matsuzaki,* Akira Ichiyanagi,† and Tomihiko Yoshida†
Nagoya University, Nagoya 464-8603, Japan

An extension of our previous analyses on the soft docking of adaptive space structures based on the artificial potential method is presented. In the previous studies of improving the artificial potential and the damping control input of the artificial potential method, we proposed control laws for the point-to-point movement of the end effector of both a space robot and a variable-geometry truss structure. Motion control is proposed to further improve the artificial potential method by taking into account a desired velocity schedule in the artificial potential. Numerical simulation has shown that the proposed method is very effective in controlling the end effector when docking a target in a soft and smooth way along an assigned straight path with no precontact.

Nomenclature

$\boldsymbol{a}_k$ = vector from joint h_k to mass center c_k
$\boldsymbol{b}_k$ = vector from mass center c_k to the origin of sliding coordinate s_{k+1}
f_k = sliding force applied to control s_k; Eq. (1b)
$\boldsymbol{J}^*$ = generalized Jacobian matrix (GJM); Eq. (4)
$\boldsymbol{J}_p^*$ = submatrix $(2 \times 2n)$ of GJM; Eq. (4)
$\boldsymbol{J}_\phi^*$ = submatrix $(1 \times 2n)$ of GJM; Eq. (4)
$\boldsymbol{K}_d$ = positive definite diagonal; Eq. (15)
$\boldsymbol{K}_v$ = positive definite symmetric matrix for damping input; Eq. (10)
$\boldsymbol{M}^*$ = inertia matrix of adaptive structure; Eq. (7)
$\boldsymbol{p}_d$ = desired state vector of $\boldsymbol{p}_h$
$\boldsymbol{p}_h$ = position vector of endpoint of link n
$\boldsymbol{p}_k$ = position vector of joint h_k
$\boldsymbol{Q}$ = control force vector, corresponding to $\boldsymbol{q}$; Eq. (1b)
$\boldsymbol{q}$ = generalized coordinate vector of joints; Eq. (1a)
$\boldsymbol{q}_d$ = desired state vector of $\boldsymbol{q}$
$\boldsymbol{r}_k$ = position vector of mass center of the link k
s = number of degrees of freedom of $\boldsymbol{q}$ for closed-link structure
s_k = sliding of joint h_k; Eq. (1a)
T = kinetic energy; Eq. (11b)
$\boldsymbol{u}$ = additional or damping input; Eq. (10)
$\bar{V}$ = artificial potential energy; Eq. (8)
$\bar{V}_p$ = component of $\bar{V}$; Eq. (17b)
$\bar{V}_\phi$ = component of $\bar{V}$; Eq. (17c)
$\boldsymbol{v}_d$ = desired translational velocity; Eq. (21)
$\boldsymbol{v}_h$ = translational velocity vector of endpoint of hand; Eq. (4)
W = Lyapunov function; Eq. (11b)
$\boldsymbol{w}_d$ = desired state vector of $\boldsymbol{w}_h$
$\boldsymbol{w}_h$ = state, i.e., position and angle vector of endpoint of hand; Eq. (3)
θ_k = rotation of joint h_k; Eq. (1a)
τ_k = torque applied to control θ_k; Eq. (1b)
ϕ_d = desired angle of ϕ_h
ϕ_h = attitude angle of link n measured from x coordinate
ω_d = desired angular velocity; Eq. (21)
ω_h = angular velocity of link n, $\dot{\phi}_h$

Presented as Paper 97-1259 at the AIAA/ASME/ASCE/AHS/ASC 38th Structures, Structural Dynamics, and Materials Conference, Kissimmee, FL, April 7–10, 1997; received May 7, 1997; revision received March 2, 1998; accepted for publication March 7, 1998.

*Professor, Department of Aerospace Engineering, Chikusa. Associate Fellow AIAA.
†Graduate Student, Department of Aerospace Engineering, Chikusa.

Introduction

DESIGN restrictions on space structures and requirements for their efficient performance inevitably lead to the emergence of adaptive space structures concepts. One such concept is the variable-geometry truss (VGT) structure.[1] That is, the truss structure changes and controls its geometrical configuration according to missions, which are given at different operational phases. A space robot with a manipulator of a serially linked type is a simple example of the VGT structure. A truss-type or closed-link variable structure, such as shown in Fig. 1, is a more capable adaptive structure.[2] Many studies have been done to apply adaptive structures concepts to controls of a variety of space structures, e.g., Refs. 2–5.

In the late 1980s many researchers carried out theoretical analyses to develop free-floating space robotic systems. A brief review of technical advancement and difficulties of space robots is included in Ref. 6. One major difficulty in controlling the motion of space robots is that the motions of the base structure, e.g., robot body, and the substructure, e.g., manipulator, floating in space are interactive, so that the motion of the manipulator influences the location and the attitude angle of the robot body and vice versa. This is not the case for a robot fixed to the ground. The components in the generalized Jacobian matrix[7] (GJM), which defines the relationship between the velocity vectors of the end effector, e.g., hand, and the joints of the truss members of the free-floating structure, change their values with time in the process of motion. In computational analyses, therefore, the GJM must be recalculated at each iteration of numerical calculation. To analyze control of the manipulator of space robots, the resolved motion rate control (RMRC) and the resolved acceleration control (RAC) have been used in, for example, Refs. 8 and 9, respectively. The RMRC and RAC are, however, very time consuming because inversion of the GJM is necessary at each computational iteration. On the other hand, the artificial potential method (APM), proposed originally by Takegaki and Arimoto,[10] needs only transpositions of the GJM, so that computation is simple and efficient. A serious drawback of the original APM was that no path of the end effector to a target can be assigned beforehand. It is often very important to accurately adjust the approaching direction to minimize misalignment and contact force between the end effector and the target. Hence, Matsuzaki et al.[4] proposed improvements on the original control laws, so that the hand or end effector may approach a target along an assigned straight path and contact it with an assigned attitude and zero terminal speed. For the prevention of interactive motions of the base structure and substructure, Matsuzaki and Tanaka[5] proposed improved control laws so that the attitude angle of the base structure can be kept constant while the end-effector may move along an assigned straight path to the contact point.

At a final stage of the soft docking operation, it is very important to avoid any precontact between the target and end effector before an assigned final contact is made because the precontact induces undesired dynamic shocks and disturbances to the target and to the

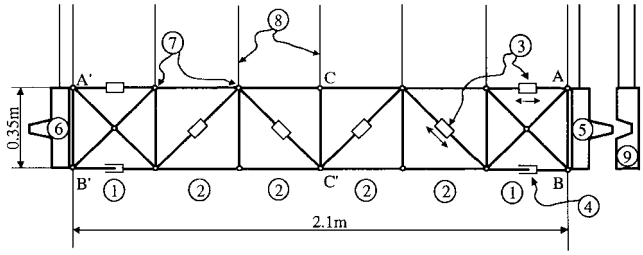

Fig. 1 Two-dimensional truss structure of variable geometry[2,3]: 1, bending deformation module; 2, shear deformation module; 3, linear actuator; 4, sliding device; 5 and 6, docking mechanism part; 7, pin joint; 8, steel wire; and 9, docking target.

docking structure itself. To avoid such a precontact, we will further develop the APM so that the velocity of the end effector can be adjusted while the end effector moves along a straight path to the target. In other words, we introduce a time schedule for this control operation.

We summarize the dynamics of a serially linked space structure and the APM described in Refs. 4, 10, and 11 and propose a motion control law. To demonstrate the effectiveness of the motion control, numerical analyses on the soft docking of a serially linked structure and a truss-type structure are presented.

Governing Equations of Serially Linked Space Structure

We assume that the docking structure and the target are constrained on the same plane. In other words, we treat a two-dimensional motion of the two-dimensional structure. Figure 2 shows the inertial coordinates and a schematic view of the serially linked space structure consisting of $(n+1)$ links, that is, a body, $(n-1)$ arms, and a hand, i.e., an end effector. Each joint possesses two degrees of freedom (DOFs), i.e., the link k has sliding s_k along the direction $\boldsymbol{n}_k$ and rotation θ_k about the joint h_k, whereas β_k and γ_k are fixed. The system under consideration has totally $2n$ DOFs. We introduce the generalized coordinate vector $\boldsymbol{q}$ of the joints and the corresponding control force vector $\boldsymbol{Q}$, which are, respectively, defined by

$$\begin{aligned}\boldsymbol{q} &= (q_1, q_2, \ldots, q_{2n})^T \\ &= (\theta_1, \theta_2, \ldots, \theta_n, s_1, s_2, \ldots, s_n)^T \qquad (1a)\\ \boldsymbol{Q} &= (Q_1, Q_2, \ldots, Q_{2n})^T \\ &= (\tau_1, \tau_2, \ldots, \tau_n, f_1, f_2, \ldots, f_n)^T \qquad (1b)\end{aligned}$$

The position vector $\boldsymbol{p}_h$ of the endpoint of the link n is given by

$$\boldsymbol{p}_h = \boldsymbol{p}_n + \boldsymbol{a}_n + \boldsymbol{b}_n \qquad (2)$$

The state vector of the endpoint, $\boldsymbol{w}_h$, is given by

$$\boldsymbol{w}_h = \begin{Bmatrix}\boldsymbol{p}_h \\ \phi_h\end{Bmatrix} \qquad (3)$$

The motion of the endpoint is, therefore, given by

$$\dot{\boldsymbol{w}}_h = \begin{bmatrix}\boldsymbol{v}_h \\ \omega_h\end{bmatrix} = \begin{bmatrix}\boldsymbol{J}_p^* \\ \boldsymbol{J}_\phi^*\end{bmatrix}\dot{\boldsymbol{q}} = \boldsymbol{J}^*\dot{\boldsymbol{q}} \qquad (4)$$

where $\boldsymbol{J}^*$ is the GJM[7] and

$$\boldsymbol{v}_h = \dot{\boldsymbol{p}}_h, \qquad \omega_h = \omega_0 + \sum_{i=1}^{n}\dot{\theta}_i \qquad (5)$$

In deriving Eq. (4), we have used the relationship between $\dot{\boldsymbol{q}}$ and the motion of the base, $\dot{\boldsymbol{w}}_0$, given by

$$\dot{\boldsymbol{w}}_0 = \begin{bmatrix}\boldsymbol{v}_0 \\ \omega_0\end{bmatrix} = -\begin{bmatrix}\boldsymbol{G}_{p_0} \\ \boldsymbol{G}_{\phi_0}\end{bmatrix}\dot{\boldsymbol{q}} \qquad (6)$$

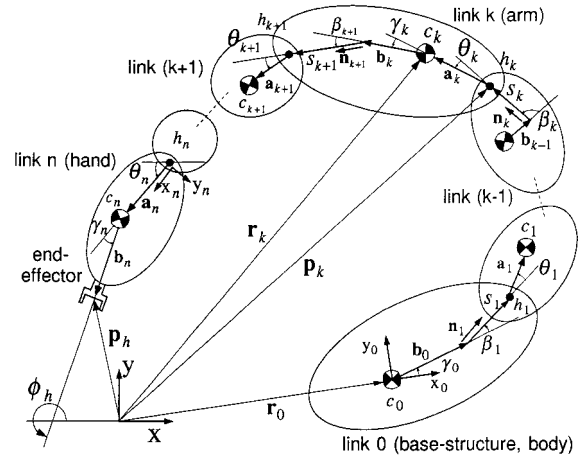

Fig. 2 Inertial coordinates and serially linked adaptive structure consisting of $(n+1)$ links.

We also assume that $\boldsymbol{J}^*$ is kept nonsingular. Singular attitude avoidance controls are treated in Refs. 12 and 13. Here $\boldsymbol{w}_h$ is a task-oriented vector and is controlled to approach a desired state $\boldsymbol{w}_d$ along an assigned straight path.

The equation of motion of the serially linked space structure is given by[7]

$$\boldsymbol{M}^*\ddot{\boldsymbol{q}} + \dot{\boldsymbol{M}}^*\dot{\boldsymbol{q}} - \frac{\partial}{\partial \boldsymbol{q}}\left(\frac{1}{2}\dot{\boldsymbol{q}}^T\boldsymbol{M}^*\dot{\boldsymbol{q}}\right) = \boldsymbol{Q} \qquad (7)$$

The docking structure is assumed to have moved to some desirable position, for instance, by a thruster installed on the base structure, so that the target is within the full stretch of the manipulator and the approach to the target is not hindered by any obstacle. To ensure accurate control of the whole docking structure, thruster force is no longer used, so that the conservation of both translational and angular momenta of the whole docking structure is held.

Control Analysis

Point-to-Point Control Based on the APM

In Ref. 4 using the APM,[10,11] we exploited a point-to-point control in which the endpoint moved along the straight path from an initial position to a contact point of the target. We briefly summarize the original APM[10,11] and the point-to-point control.[4]

Introducing an artificial potential energy $\bar{V}(\boldsymbol{q})$, we may express the control input force as

$$\boldsymbol{Q} = -\frac{\partial \bar{V}}{\partial \boldsymbol{q}} + \boldsymbol{u} \qquad (8)$$

where $\boldsymbol{u}$ is an additional input. $\bar{V}(\boldsymbol{q})$ is positive definite and satisfies

$$\begin{aligned}&\bar{V}(\boldsymbol{q}) > 0 \qquad \text{for} \qquad \boldsymbol{q} \neq \boldsymbol{q}_d \\ &\bar{V}(\boldsymbol{q}) = \frac{\partial \bar{V}(\boldsymbol{q})}{\partial \boldsymbol{q}} = 0 \qquad \text{for} \qquad \boldsymbol{q} = \boldsymbol{q}_d\end{aligned} \qquad (9)$$

If the additional input $\boldsymbol{u}$ is given by

$$\boldsymbol{u} = -\boldsymbol{K}_v\dot{\boldsymbol{q}} \qquad (10)$$

where $\boldsymbol{K}_v$ is a positive definite symmetric matrix, then the time derivative of the Lyapunov function W is reduced to[10]

$$\dot{W} = -\dot{\boldsymbol{q}}^T\boldsymbol{K}_v\dot{\boldsymbol{q}} < 0 \qquad \text{for} \qquad \dot{\boldsymbol{q}} \neq 0 \qquad (11a)$$

where

$$W = T + \bar{V} \qquad (11b)$$

It follows from Eqs. (7–10) that $\ddot{\boldsymbol{q}} = \dot{\boldsymbol{q}} = \boldsymbol{0}$ only if $\boldsymbol{q} = \boldsymbol{q}_d$. Because $\dot{W}$ is negative definite, the controlled system is asymptotically stable; that is, the joint state vector $\boldsymbol{q}$ approaches the desired $\boldsymbol{q}_d$ for any $\bar{V}$. In other words, the velocity feedback given by Eq. (10) works as a stabilizing and damping force. Furthermore, it may be proved

from the Lyapunov–Bellmann optimality condition[14] that the performance index (PI), which is defined by

$$\mathrm{PI} = \int_0^\infty \frac{1}{2}\left(\dot{\boldsymbol{q}}^T \boldsymbol{K}_v \dot{\boldsymbol{q}} + \boldsymbol{u}^T \boldsymbol{K}_v^{-1} \boldsymbol{u}\right) \mathrm{d}t \tag{12}$$

becomes minimized through the damping control input defined by Eq. (10). Therefore, the control based on Eq. (10) is optimal in the sense that Eq. (12) is minimized.

In the optimally controlled system governed by Eqs. (7), (8), and (10), the state vector of the joint $\boldsymbol{q}$ approaches the desired $\boldsymbol{q}_d$ while its velocity $\dot{\boldsymbol{q}}$ approaches $\dot{\boldsymbol{q}}_d = \boldsymbol{0}$. At the terminal state, no control input force is applied, i.e., $\boldsymbol{Q} = \boldsymbol{0}$. It is useful to express the artificial potential in terms of the task-oriented coordinate vector $\boldsymbol{w}_h$ because $\boldsymbol{w}_h$ is required to approach $\boldsymbol{w}_d$. As the free-floating space adaptive structure is a nonholonomic system, the relationship between $\boldsymbol{w}_h$ and $\boldsymbol{q}$ is not unique, and Eq. (4) governs the velocity relation between $\dot{\boldsymbol{w}}_h$ and $\dot{\boldsymbol{q}}$. Nevertheless, because the variance in $\boldsymbol{J}^*$ is very small in a short period, we assume during each numerical iteration of a short step that

$$\boldsymbol{J}^* = \frac{\partial \boldsymbol{w}_h}{\partial \boldsymbol{q}} \tag{13}$$

As shown in Refs. 4 and 5, we have confirmed that the artificial potential $\bar{V}$ expressed in terms of $\boldsymbol{w}_h$ may possess an asymptotic stability toward $\boldsymbol{w}_d$. The input control force can be given as

$$\boldsymbol{Q} = -\boldsymbol{J}^{*T}\left(\frac{\partial \bar{V}(\boldsymbol{w}_h)}{\partial \boldsymbol{w}_h}\right)^T + \boldsymbol{u} \tag{14}$$

In the following, without loss of generality, we assume that each joint has only one DOF, that is, the rotation about its joint is included but no sliding, so that the dimensions of $\boldsymbol{q}$ and $\boldsymbol{Q}$ given by Eqs. (1) become n instead of $2n$. Additionally, the manipulator is assumed to be nonredundant, namely, $n = 3$ for the in-plane motion.

Like in Refs. 4 and 11, if the damping coefficient matrix $\boldsymbol{K}_v$ in Eq. (10) is simply a positive definite diagonal such as defined by

$$\boldsymbol{K}_v = \boldsymbol{K}_d \tag{15a}$$

where

$$\boldsymbol{K}_d = \mathrm{diag}[k_1 \;\; k_2 \;\; k_3] \qquad \text{with} \qquad k_i > 0 \qquad \text{for} \qquad i = 1, 2, 3 \tag{15b}$$

then the path taken by the end effector to the target point cannot be assigned beforehand although it finally reaches the point, as proved earlier.

For the point-to-point control with a straight path, Matsuzaki et al.[4] have presented two control laws: One elaborated on the damping input $\boldsymbol{u}$ and the other on the artificial potential $\bar{V}$. We describe the former control.

The damping coefficient matrix proposed in Ref. 4 is expressed in terms of $\boldsymbol{J}^*$ as

$$\boldsymbol{K}_v = \boldsymbol{J}^{*T} \boldsymbol{K}_d \boldsymbol{J}^* \tag{16}$$

The artificial potential energy is given by[4]

$$\bar{V} = \bar{V}_p + \bar{V}_\phi \tag{17a}$$

where

$$\bar{V}_p = \begin{cases} \frac{1}{2} k_p (\boldsymbol{p}_d - \boldsymbol{p}_h)^T (\boldsymbol{p}_d - \boldsymbol{p}_h), & \|\boldsymbol{p}_d - \boldsymbol{p}_h\| \le e_{p\max} \\ k_p e_{p\max} \sqrt{(\boldsymbol{p}_d - \boldsymbol{p}_h)^T (\boldsymbol{p}_d - \boldsymbol{p}_h)} - \frac{1}{2} k_p e_{p\max}^2, & \|\boldsymbol{p}_d - \boldsymbol{p}_h\| > e_{p\max} \end{cases} \tag{17b}$$

$$\bar{V}_\phi = \begin{cases} \frac{1}{2} k_\phi (\phi_d - \phi_h)^2, & |\phi_d - \phi_h| \le e_{\phi\max} \\ k_\phi e_{\phi\max} |\phi_d - \phi_h| - \frac{1}{2} k_\phi e_{\phi\max}^2, & |\phi_d - \phi_h| > e_{\phi\max} \end{cases} \tag{17c}$$

The potential $\bar{V}$ represents a penalty for the difference between the actual and the desired state of the endpoint.

Substitution of Eqs. (10), (16), and (17) into Eq. (14) yields

$$\boldsymbol{Q} = \boldsymbol{J}_p^{*T} k_p \boldsymbol{e}_p + \boldsymbol{J}_\phi^{*T} k_\phi e_\phi - \boldsymbol{J}^{*T} \boldsymbol{K}_d \boldsymbol{J}^* \dot{\boldsymbol{q}} \tag{18a}$$

where

$$\boldsymbol{e}_p = \begin{cases} \boldsymbol{p}_d - \boldsymbol{p}_h, & \|\boldsymbol{p}_d - \boldsymbol{p}_h\| \le e_{p\max} \\ \dfrac{e_{p\max}}{\|\boldsymbol{p}_d - \boldsymbol{p}_h\|}(\boldsymbol{p}_d - \boldsymbol{p}_h), & \|\boldsymbol{p}_d - \boldsymbol{p}_h\| > e_{p\max} \end{cases} \tag{18b}$$

$$e_\phi = \begin{cases} \phi_d - \phi_h, & |\phi_d - \phi_h| \le e_{\phi\max} \\ \dfrac{e_{\phi\max}}{|\phi_d - \phi_h|}(\phi_d - \phi_h), & |\phi_d - \phi_h| > e_{\phi\max} \end{cases} \tag{18c}$$

To avoid excessive inputs, the upper limit has been assigned to the input by $e_{p\max}$ and $e_{\phi\max}$. Substitution of Eqs. (10) and (16) together with Eq. (4) into Eq. (12) yields

$$\mathrm{PI} = \int_0^\infty \dot{\boldsymbol{w}}_h^T \boldsymbol{K}_d \dot{\boldsymbol{w}}_h \, \mathrm{d}t \tag{19}$$

which is minimized for the damping input based on Eq. (16). Because the cumulative deviation of the quadratic form of $\dot{\boldsymbol{w}}_h(t)$ becomes the minimum, the endpoint moves along a straight path from the initial position to the contact point. If $\boldsymbol{v}_h(t)$ has any component normal to the straight path, then the PI will clearly not be minimized. Similarly, the rotation is required to have little unnecessary motion. If k_1, k_2, and k_3 are set to sufficiently large values, then the endpoint will take a path that is very close to the straight path. The control described here will be called control 1.

Motion Control for the APM

In control 1, the control force based on both the artificial potential and the damping input guarantees an asymptotically stable and optimal straight-path approach to the docking target. As the artificial potential simply represents a penalty for the deviation of the actual state of the endpoint from the desired one, if the feedback gains of the potential, k_p and k_ϕ, are very large, then they will deteriorate the effect of the damping input for controlling the endpoint to move along the assigned straight path. This is because the effect of the artificial potential becomes predominant, so that the endpoint might not avoid a precontact with some part of the target. It is not a simple matter to select an appropriate combination of the gains for the artificial potential and the damping input. To avoid precontact in a more direct manner, we propose a motion control of the endpoint for which the artificial potential contains not only the deviation from the desired state of the endpoint but also a desired velocity schedule.

Using the same damping control as used in control 1, that is,

$$\boldsymbol{u} = -\boldsymbol{J}^{*T} \boldsymbol{K}_d \boldsymbol{J}^* \dot{\boldsymbol{q}} = -\boldsymbol{J}^{*T} \boldsymbol{K}_d \dot{\boldsymbol{w}}_h \tag{20}$$

we propose a control input force given by

$$\boldsymbol{Q} = -k_1 \boldsymbol{J}_p^{*T} \boldsymbol{v}_h - k_3 \boldsymbol{J}_\phi^{*T} \omega_h + k_p \boldsymbol{J}_p^{*T} \left[v_d(\|\boldsymbol{p}_d - \boldsymbol{p}_h\|) \frac{\boldsymbol{p}_d - \boldsymbol{p}_h}{\|\boldsymbol{p}_d - \boldsymbol{p}_h\|} \right]$$
$$+ k_\phi \boldsymbol{J}_\phi^{*T} \left[\omega_d(|\phi_d - \phi_h|) \frac{\phi_d - \phi_h}{|\phi_d - \phi_h|} \right] \tag{21}$$

where functions $v_d(\|\boldsymbol{p}_d - \boldsymbol{p}_h\|)$ and $\omega_d(|\phi_d - \phi_h|)$ represent magnitudes of the desired translational and angular velocities, which are, respectively, at a distance of $\|\boldsymbol{p}_d - \boldsymbol{p}_h\|$ from the target point and at an angle $|\phi_d - \phi_h|$ from the desired one; and k_2 has been assumed to be equal to k_1.

In the present approach, the feedback gains $k_1 = k_2$ and k_3 for the damping input are set to sufficiently large values, so that the endpoint will move along the assigned straight path. In other words, the endpoint has the translational and angular velocities toward the target, i.e.,

$$\boldsymbol{v}_h \cong \|\boldsymbol{v}_h\| \frac{\boldsymbol{p}_d - \boldsymbol{p}_h}{\|\boldsymbol{p}_d - \boldsymbol{p}_h\|}, \qquad \omega_h \cong |\omega_h| \frac{\phi_d - \phi_h}{|\phi_d - \phi_h|} \tag{22}$$

As we may expect that $\boldsymbol{Q} = \dot{\boldsymbol{q}} = \dot{\boldsymbol{w}}_h = \boldsymbol{0}$ is satisfied at the terminal state, by setting

$$k_p = k_1, \qquad k_\phi = k_3 \tag{23}$$

and substituting Eqs. (22) into Eq. (21), we obtain

$$\|\boldsymbol{v}_h\| = v_d, \qquad |\omega_h| = \omega_d \tag{24}$$

at $\boldsymbol{w}_h = \boldsymbol{w}_d$. In other words, the absolute values of the translational and angular velocities of the endpoint are equal to the desired amounts of velocity values at the terminal state.

Next, we obtain the artificial potential by integrating the last two terms in the right-hand side of Eq. (21):

$$\bar{V}(\boldsymbol{w}_h) = -k_1 \int \left(v_d \frac{\boldsymbol{p}_d - \boldsymbol{p}_h}{\|\boldsymbol{p}_d - \boldsymbol{p}_h\|} \right) \mathrm{d}\boldsymbol{p}_h - k_3 \int \left(\omega_d \frac{\phi_d - \phi_h}{|\phi_d - \phi_h|} \right) \mathrm{d}\phi_h \tag{25}$$

$\bar{V}(\boldsymbol{w}_h)$ satisfies the positiveness, Eqs. (9), i.e.,

$$\begin{aligned} \bar{V}(\boldsymbol{w}_h) &> 0 \qquad \text{for} \qquad \boldsymbol{w}_h \neq \boldsymbol{w}_d \\ \bar{V}(\boldsymbol{w}_h) &= 0 \qquad \text{for} \qquad \boldsymbol{w}_h = \boldsymbol{w}_d \end{aligned} \tag{26}$$

The introduction of the desired velocity schedule based on v_d and ω_d will make it possible to control the endpoint to approach the target point with the desired terminal velocity. Hence, the possibility of precontact is much reduced. We call the control law based on Eq. (21) control 2.

In controls 1 and 2, we have assumed that the number of DOFs of the manipulator, n, is equal to 3, that is, the number of the state variables of the endpoint. To adaptively perform different types of missions, it is more suitable for the manipulator to have a greater number of DOFs than 3, that is, a redundancy. It is rather easy to extend controls 1 and 2 to such a redundant manipulator using, for instance, an augmented GJM.

Motion Control of Closed-Link Space Structure

In a closed-link structure, such as shown in Fig. 1, all of the state variables of the vector $\boldsymbol{q}$ are not necessarily independent. Now we regain the DOFs for sliding of the link members, so that the dimensions of $\boldsymbol{q}$ and $\boldsymbol{Q}$ are $2n$. Let the number of DOFs of $\boldsymbol{q}$ be s and the independent state vector and the corresponding control force vector be $\tilde{\boldsymbol{q}}$ and $\tilde{\boldsymbol{Q}}$, respectively, which are defined by

$$\tilde{\boldsymbol{q}} = (\tilde{q}_1, \tilde{q}_2, \ldots, \tilde{q}_s)^T, \qquad s < 2n \tag{27}$$

$$\tilde{\boldsymbol{Q}} = (\tilde{Q}_1, \tilde{Q}_2, \ldots, \tilde{Q}_s)^T, \qquad s < 2n \tag{28}$$

The state vector $\boldsymbol{q}$ can be expressed in terms of $\tilde{\boldsymbol{q}}$ as

$$\boldsymbol{q} = \Psi(\tilde{\boldsymbol{q}}) = [\psi_1(\tilde{\boldsymbol{q}}), \psi_2(\tilde{\boldsymbol{q}}), \ldots, \psi_{2n}(\tilde{\boldsymbol{q}})]^T \tag{29}$$

Introducing Eq. (29) into Eq. (4), we obtain

$$\dot{\boldsymbol{w}}_h = \tilde{\boldsymbol{J}}^* \dot{\tilde{\boldsymbol{q}}} \tag{30}$$

where $\tilde{\boldsymbol{J}}^*$ is an equivalent GJM defined by

$$\tilde{\boldsymbol{J}}^* = \boldsymbol{J}^* \Gamma, \qquad \in R^{3 \times s} \tag{31}$$

$$\Gamma = \begin{bmatrix} \dfrac{\partial \psi_1}{\partial \tilde{q}_1} & \cdots & \dfrac{\partial \psi_1}{\partial \tilde{q}_s} \\ \vdots & \ddots & \vdots \\ \dfrac{\partial \psi_{2n}}{\partial \tilde{q}_1} & \cdots & \dfrac{\partial \psi_{2n}}{\partial \tilde{q}_s} \end{bmatrix}, \qquad \in R^{2n \times s} \tag{32}$$

Using Eqs. (27–30), we may finally obtain the governing equation of the closed-link structure such as Eq. (7):

$$\tilde{\boldsymbol{M}}^* \ddot{\tilde{\boldsymbol{q}}} + \dot{\tilde{\boldsymbol{M}}}^* \dot{\tilde{\boldsymbol{q}}} - \frac{\partial}{\partial \tilde{\boldsymbol{q}}} \left(\frac{1}{2} \dot{\tilde{\boldsymbol{q}}}^T \tilde{\boldsymbol{M}}^* \dot{\tilde{\boldsymbol{q}}} \right) = \tilde{\boldsymbol{Q}} \tag{33}$$

where

$$\tilde{\boldsymbol{M}}^* = \Gamma^T \boldsymbol{M}^* \Gamma \tag{34}$$

Now we may apply controls 1 and 2 similarly to the motion of the closed-link structure given by Eq. (33).

Numerical Analysis

To examine the effectiveness of the proposed control law for docking a target, we have carried out numerical simulations of the motion of a serially linked space robot and a truss-type structure. Some typical results will be shown in the following.

Figure 3a shows a schematic picture of the robot consisting of a body, two arms, and a hand, which are located at the initial position, and the contact point of the target. The assigned attitude of the hand to the target point is shown by a thick arrow. In this numerical analysis, the docking target is representatively expressed with a point on a wall fixed to the inertial coordinate, and we study the soft docking in which the endpoint reaches the target along an assigned straight path with zero final relative velocity without any precontact with the wall. In other words, any precontact simply means a failure of the soft docking. Even though the endpoint contacted the wall with a nonzero relative speed, the computation was continued on a condition that no reactive force and no interactive motions between the hand and the wall were considered. That is, the precontact between the wall and the endpoint did not influence the motion of the endpoint. A precontact will be expressed as a negative distance between the endpoint and the target point. Numerical values of the parameters of the links used in the calculation are given in Table 1. Parameter values used in the control input are given in Table 2. The governing equations were solved for numerical iteration of $\Delta t = 0.1$ s. In Figs. 3b and 3c, the progressive motions of the robot calculated by using controls 1 and 2, respectively, are illustrated at a time interval

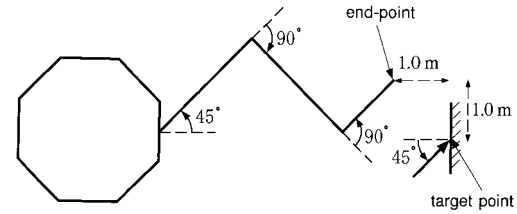

Fig. 3a Initial position of robot and target point.

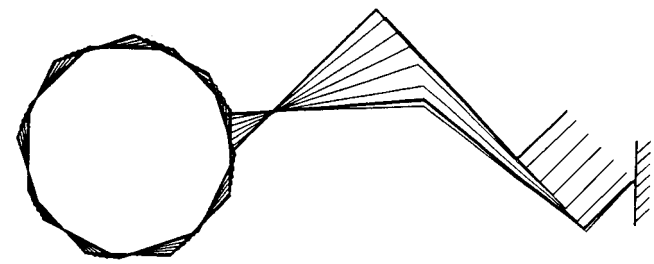

Fig. 3b Progressive motion by control 1.

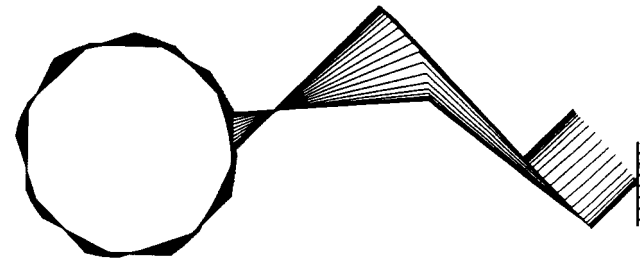

Fig. 3c Progressive motion by control 2.

Table 1 Numerical values of parameters of links: manipulator

Link no.	m_k, kg	I_k, kgm^2	Length, m
0	1500.0	1500.0	3.0
1	50.0	30.0	3.0
2	50.0	30.0	3.0
3	15.0	10.0	1.0

Table 2 Control gains

Control	k_p	k_ϕ	k_1	k_2	k_3	$e_{p\max}$	$e_{\phi\max}$
			Manipulator				
1	180.0	180.0	200.0	200.0	200.0	0.1	0.1
2	180.0	180.0	——	——	——	——	——
			Truss				
1	20.0	30.0	250.0	250.0	150.0	0.2	0.1
2	180.0	180.0	——	——	——	——	——

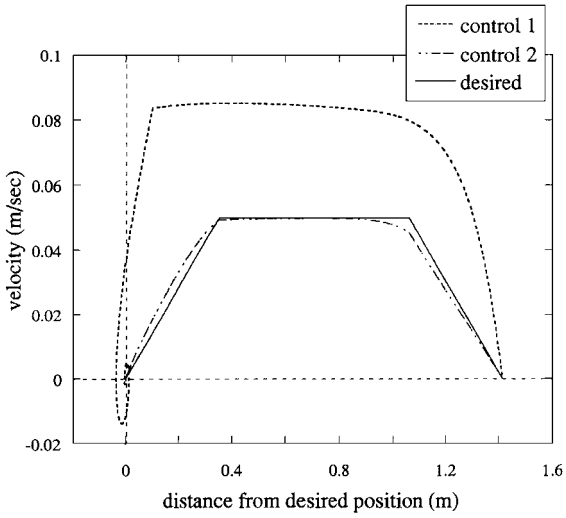

Fig. 4a Velocity vs distance (manipulator).

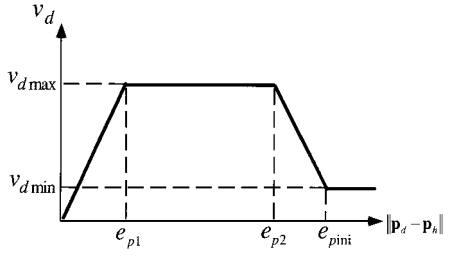

Fig. 4b Desired velocity vs distance.

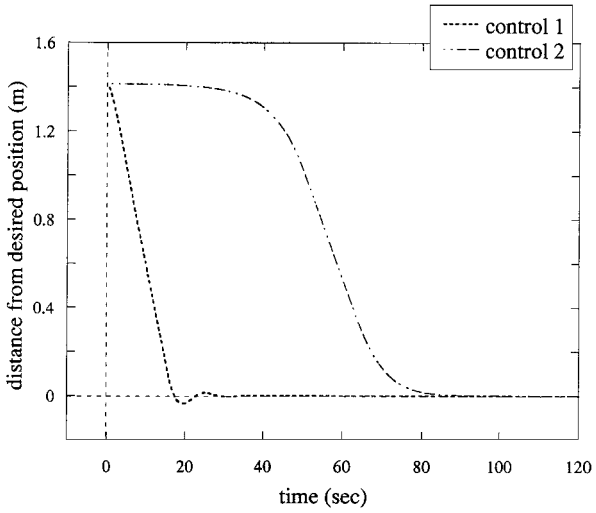

Fig. 4c Distance vs time.

of 3 s. It is clear that the endpoint took a straight path to the target point in each control. It should be noted here that, when the damping matrix $\boldsymbol{K}_v$ was given by Eq. (15) as in the original APM,[10,11] the path taken by the endpoint was unpredictable and curved,[15] as shown in Fig. 4b of Ref. 4. In Fig. 4a here, the desired translational velocity schedule is shown by a solid line against the distance between the endpoint and the contact point, i.e., $\|\boldsymbol{p}_d - \boldsymbol{p}_h\|$. The artificial potential $\bar{V}_p$ that satisfies the desired velocity schedule is given from Eq. (25) as

$$\frac{\bar{V}_p}{k_p} = \begin{cases} \frac{1}{2}\frac{v_{d\max}}{e_{p1}}(\boldsymbol{p}_d - \boldsymbol{p}_h)^T(\boldsymbol{p}_d - \boldsymbol{p}_h), & (\|\boldsymbol{p}_d - \boldsymbol{p}_h\| \le e_{p1}) \\ C_{p1} + v_{d\max}\|\boldsymbol{p}_d - \boldsymbol{p}_h\|, & (e_{p1} < \|\boldsymbol{p}_d - \boldsymbol{p}_h\| \le e_{p2}) \\ C_{p2} + (v_{d\max} + e_{p2}C_{p3})\|\boldsymbol{p}_d - \boldsymbol{p}_h\| - \frac{1}{2}C_{p3}\|\boldsymbol{p}_d - \boldsymbol{p}_h\|^2 & \\ \qquad (e_{p2} < \|\boldsymbol{p}_d - \boldsymbol{p}_h\| \le e_{p\,\mathrm{ini}}) & \\ C_{p4} + v_{d\min}\|\boldsymbol{p}_d - \boldsymbol{p}_h\|, & (e_{p\,\mathrm{ini}} < \|\boldsymbol{p}_d - \boldsymbol{p}_h\|) \end{cases} \tag{35}$$

where

$$C_{p1} = -\tfrac{1}{2}v_{d\max}e_{p1}, \qquad C_{p2} = -\tfrac{1}{2}v_{d\max}e_{p1} + \tfrac{1}{2}C_{p3}e_{p2}^2$$

$$C_{p3} = \frac{v_{d\max} - v_{d\min}}{e_{p\,\mathrm{ini}} - e_{p2}}$$

$$C_{p4} = v_{d\max}\left(-\tfrac{1}{2}e_{p1} + e_{p\,\mathrm{ini}}\right) - \tfrac{1}{2}C_{p3}(e_{p2} - e_{p\,\mathrm{ini}})^2 - v_{d\min}e_{p\,\mathrm{ini}}$$

The definitions of the parameters in the preceding equations are shown in Fig. 4b here. As the initial and the assigned final attitude of the hand were parallel, we assigned ω_d to zero in the angular velocity schedule. Numerical values used in the simulation are given in Table 3.

The translational velocities of the endpoint controlled by controls 1 and 2 are, respectively, shown by dot and dot–dash curves in Fig. 4a, whereas the distance between the endpoint and the contact point is plotted against time in Fig. 4c, where dot and dot–dash

Table 3 Numerical values of desired velocity parameters

e_{p1}	e_{p2}	$e_{p\,\mathrm{ini}}$	$v_{d\max}$	$v_{d\min}$	e_{f1}	e_{f2}	$e_{f\,\mathrm{ini}}$	$w_{d\max}$	$w_{d\min}$
0.3536	1.0607	1.4142	0.05	0.0001	11.25	33.75	45.0	2.0	0.01

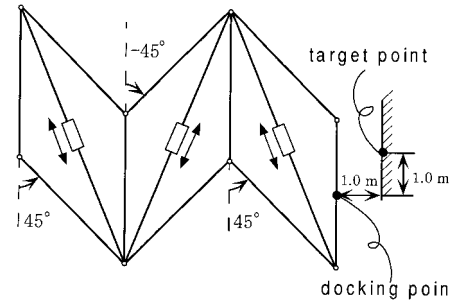

Fig. 5a Initial state of truss structure.

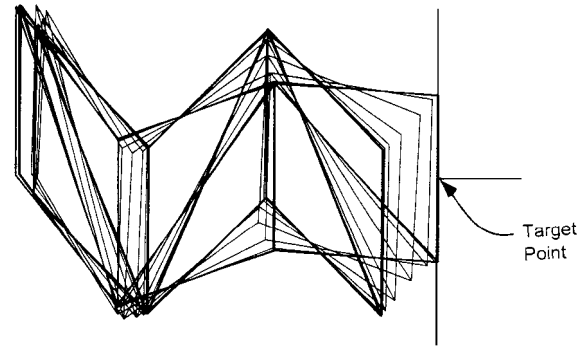

Fig. 5b Progressive motion by control 2.

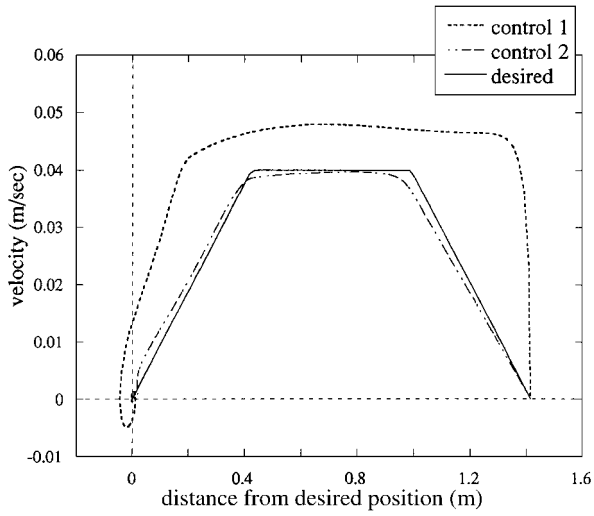

Fig. 6a Velocity vs distance (truss).

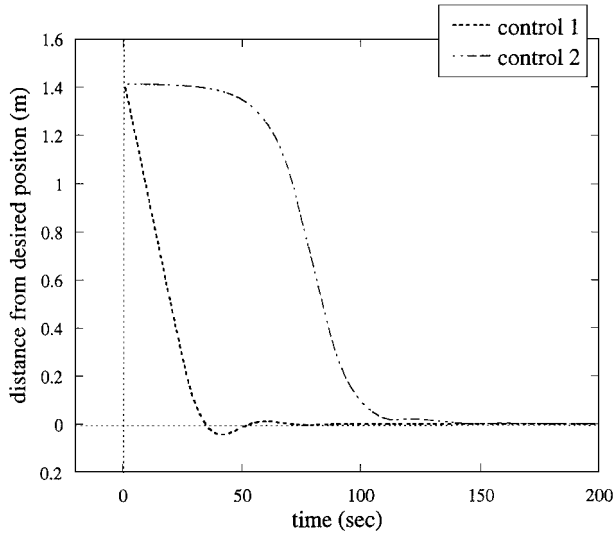

Fig. 6b Distance vs time.

curves represent controls 1 and 2, respectively. The endpoint controlled by control 1 underwent a precontact. The distance given by the dot curve is negative between t equal to about 17 and 23 s in Fig. 4c, and the dot curve crosses the vertical velocity coordinate at a value of about 0.035 m/s in Fig. 4a. On the other hand, control 2 was successful in completing the soft docking, as shown in Fig. 4a. It should be noted that the dot–dash curve followed well the desired velocity schedule through the whole operational process, although the velocity has theoretically been predicted to be close to the desired velocity in the neighborhood of the target point. The distance shown by the dot–dash curve decreased to zero in a very smooth manner without becoming negative in Fig. 4c. As for the soft docking of a robot with a redundant manipulator with five arms and a hand, Ichiyanagi[15] numerically demonstrated smooth contact with a target following given velocity schedule on v_d and ω_d.

Finally, we describe the motion control of a truss-type smart structure such as shown in Fig. 1. Numerical values of gains used in the calculation are also given in Table 2. As for the desired velocity parameters, the same values as given in Table 3 were used except for $v_{d\max} = 0.04$. Figure 5a shows an initial configuration of a simple pin-jointed structure with three shear modules with an extendable slant member in each module as well as a docking point located at the center of the rightmost member and a target point on a wall fixed in the inertial coordinates. The slant member consists of two uniform rods, which have a mass of 50 kg and a length of 3 m. The inertia moment of the rod is 30 kgm^2. The two rods may slide with each other smoothly through a massless sliding device. The same rod is used for the remaining 10 truss members. In Fig. 5b, a progressive motion of the structure controlled by control 2 is shown from the initial to the terminal state. Figures 6a and 6b show, respectively, the desired and actual velocities of the docking point and the distance between the docking and the target point. It is again clear that control 2 is very successful in performing the soft docking of the truss-type structure.

Concluding Remarks

We have further developed the APM for the docking control of the adaptive space structures for approaching the targets by proposing the motion control. In the new optimal control, the artificial potential is improved to include the effect of the desired velocity schedule, so that the end effector may move along the assigned straight path and dock the target with zero contact velocity and an assigned attitude. The numerical simulations have confirmed that the end effector of the robot or the adaptive truss structure may reach the target point in a soft and smooth manner with no precontact.

References

[1]Miura, K., "Adaptive Structures Research at ISAS, 1984–1990," *Journal of Intelligent Materials Systems Structures*, Vol. 3, No. 1, 1992, pp. 54–74.

[2]Matsuzaki, Y., Furuya, H., Kuwao, F., and Takahara, K., "Docking/Separation Test of Two-Dimensional Truss Structure with Variable Geometries," AIAA Paper 90-0945, April 1990.

[3]Matsuzaki, Y., and Abe, S., "Application of Neural Networks to Tracking Analysis for Rendezvous/Docking of an Adaptive Space Structure," AIAA Paper 92-2402, April 1992.

[4]Matsuzaki, Y., Miura, T., Ichiyanagi, A., and Tanaka, M., "Dynamic Control of Docking of Adaptive Space Structure Based on Artificial Potential Method," AIAA Paper 95-1087, April 1995.

[5]Matsuzaki, Y., and Tanaka, M., "Soft Docking of Adaptive Space Structures Based on Artificial Potential Method," AIAA Paper 96-1286, April 1996.

[6]Dubousky, S., and Papadopoulos, E., "The Kinematics, Dynamics, and Control of Free-Flying and Free-Floating Space Robotic System," *IEEE Transactions on Robotics and Automation*, Vol. 9, No. 5, 1993, pp. 531–543.

[7]Umetani, Y., and Yoshida, K., "Continuous Path Control of Space Manipulators Mounted on OMV," *Acta Astronautica*, Vol. 15, No. 12, 1987, pp. 981–986.

[8]Whitney, D., "Resolved Motion Rate Control of Manipulators and Human Prostheses," *IEEE Transactions, Man–Machine Systems*, Vol. MMS-10, June 1969, pp. 47–53.

[9]Luh, J. Y. S., Walker, M. W., and Paul, P. R. C., "Resolved-Acceleration Control of Mechanical Manipulators," *IEEE Transactions on Automatic Control*, Vol. 25, No. 3, 1980, pp. 468–474.

[10]Takegaki, M., and Arimoto, S., "A New Feedback Method for Dynamic Control of Manipulators," *Journal of Dynamic Systems, Measurement and Control*, Vol. 103, No. 2, 1981, pp. 119–125.

[11]Masutani, Y., and Miyazaki, F., "Sensory Feedback Control for Space Manipulators" *Transactions of Japan Robotic Society*, Vol. 7, No. 6, 1989, pp. 647–655 (in Japanese).

[12]Padopoulos, E., and Dubowsky, S., "Dynamic Singularities in Free-Floating Space Manipulators," *Journal of Dynamic Systems, Measurement and Control*, Vol. 115, March 1993, pp. 44–52.

[13]Matsuzaki, Y., and Yoshida, T., "Singular Attitude Avoidance Control of Adaptive Structure," *Proceedings of the 8th International Conference on Adaptive Structures and Technology*, Technomic, Lancaster, PA, 1998, pp. 343–352.

[14]Letov, A. M., *Stability Theory. System Theory*, edited by L. Zadeh and E. Polack, McGraw–Hill, New York, 1969, Chap. 3, Sec. 8.

[15]Ichiyanagi, A., "Path and Velocity Control by Space Manipulator," M.S. Thesis, Dept. of Aerospace Engineering, Nagoya Univ., Chikusa, Nagoya, Japan, March 1996 (in Japanese).

F. H. Lutze Jr.
Associate Editor